Journal of Sound and Vibration 568 (2024) 117961

Contents lists available at ScienceDirect

Journal of Sound and Vibration

journal homepage: www.elsevier.com/locate/jsvi

Cross-modulation in guided wave propagation: how does it relate to the Luxemburg-Gorky effect?

Shengbo Shan [a,*], Yuanman Zhang [b,c], Ze Liu [b,c], Fuzhen Wen [b], Li Cheng [b,c,d,**], Wieslaw J Staszewski [e,*]

[a] School of Aerospace Engineering and Applied Mechanics, Tongji University, Shanghai 200092, PR China
[b] Department of Mechanical Engineering, The Hong Kong Polytechnic University, Kowloon, Hong Kong, PR China
[c] The Hong Kong Polytechnic University Shenzhen Research Institute, Shenzhen 518057, PR China
[d] Hong Kong Branch of National Rail Transit Electrification and Automation Engineering Technology Research Center, The Hong Kong Polytechnic University, Kowloon, Hong Kong, PR China
[e] Department of Robotics and Mechatronics, AGH University of Science and Technology, Al. Mickiewicza 30, Krakow 30-059, Poland

ARTICLE INFO

Keywords:
Cross-modulation
The Luxemburg-Gorky effect
Guided waves
Wave mixing
Material nonlinearity

ABSTRACT

The well-known Luxemburg-Gorky effect in radio waves has also been observed in elastic waves recently, which points to new possibilities for incipient damage detection. However, how the cross-modulation phenomenon of guided waves in a weakly nonlinear medium is related to the Luxemburg-Gorky effect remains an open question. This issue is investigated in this paper. Considering the third-order nonlinear elasticity of a plate waveguide, a theoretical framework is proposed to analyze the influence of the mode combination and mixing direction of a pair of single-frequency and modulated waves on the cross-modulated component generation. In particular, a codirectional shear-horizontal wave mixing scheme is highlighted which enables the generation of internally-resonant cross-modulated components at all frequencies. After verification by finite element simulation, mechanisms underpinning the cross-modulated components in the codirectional shear-horizontal wave mixing scheme are revealed through tactical tuning of the higher-order material elastic constants. Experiments are conducted to further confirm the phenomena and substantiate their relevance to the Luxemburg-Gorky effect. It is established that the cross-modulated components of guided waves can be generated and practically measured in a weakly nonlinear plate via both pure and mixed mechanisms as a result of the cubic nonlinearity instead of the quadratic nonlinearity. Compared with the conventional two-wave mixing methods based on quadratic nonlinearity, the cross-modulated components exhibit higher sensitivity to material microstructural changes, which is conducive to incipient damage detection. Although the observed nonlinear cross-modulation in guided waves shows similarities with the Luxemburg-Gorky effect, they stem from different mechanisms: the former from nonlinear elasticity and the latter nonlinear dissipation.

* Corresponding authors.
** Corresponding author at: Department of Mechanical Engineering, The Hong Kong Polytechnic University, Kowloon, Hong Kong, PR China.
E-mail addresses: shanshengbo@tongji.edu.cn (S. Shan), li.cheng@polyu.edu.hk (L. Cheng), staszews@agh.edu.pl (W.J. Staszewski).

https://doi.org/10.1016/j.jsv.2023.117961
Received 26 February 2023; Received in revised form 9 July 2023; Accepted 22 July 2023
Available online 23 July 2023

1. Introduction

During the initiation and evolution of material damage, changes in the linear elastic modulus are usually much weaker than changes in the accompanying nonlinear parameters. Thus, nonlinear acoustics has found promising applications in material microstructure evaluation and in incipient damage detection exemplified by higher harmonics, combinational harmonics, nonlinear modulation, nonlinear demodulation, nonlinear slow dynamics, etc. Plate-like structures are widely used in industry [1,2]. Nonlinear guided waves in such structures, resulting from the primary wave interaction with material microstructural defects such as lattice anharmonicity, inclusions, voids, dislocations, and micro-cracks have received increasing attention for detecting incipient damage in many non-destructive evaluation (NDE) applications [3–8]. Depending on the combinations of primary guided waves, different types of nonlinear guided waves are generated. The most commonly used nonlinear effects of guided waves for NDE applications are higher harmonics [9–11] and mixed-frequency components induced by wave mixing [12,13].

Higher harmonics result from wave self-interaction in nonlinear plates [4,5,14], among which the second harmonic guided waves have been extensively exploited. It is shown that the second harmonic guided waves can only be generated if the power flux from the fundamental waves to the second harmonic waves is non-zero. In addition, when the phase velocities of the fundamental and second harmonic waves match, the generated nonlinear waves are cumulative with respect to the propagating distance [15,16]. Governed by the two conditions, the mode pairs that allow the cumulative second harmonic generation at some specific frequencies are identified [17] and further applied to detect incipient damage caused by fatigue [18], plastic deformation [19], and creep [20] in plates. Alternatively, the third harmonic guided waves also attract increasing attention recently [21,22]. It is found that the third harmonic SH waves are internally resonant with their fundamental counterparts and exhibit cumulative effect at all frequencies, which offers enormous flexibility for selecting the mode pairs in NDE applications [21]. Besides, the third harmonic waves have been shown to be more sensitive than the second harmonic waves to incipient damage such as fatigue [23] and thermal damage [24]. Nevertheless, due to the weak nature of the nonlinear guided waves, the higher harmonic guided waves are vulnerable to the deceptive nonlinear sources in the measurement system including the instrumentation nonlinearity, transducer nonlinearity, and adhesive nonlinearity, which may deteriorate damage detection in practical applications [25,26].

Wave mixing leverages the mutual interaction among multiple primary guided waves with different frequencies and modes in nonlinear plates to generate the mixed-frequency components [12,27–29]. As the primary waves require to be separately excited with independent physical channels, the wave mixing only takes place in the plate so that the wave mixing technique is immune to the deceptive nonlinear sources in the measurement system. In addition, the wave mixing zone and mixing angles can be flexibly tuned to target specific detection areas. For example, Hasanian and Lissenden theoretically derived internally-resonant mode combinations that satisfy both the non-zero power flux and phase matching conditions considering arbitrary wave mixing angles and quadratic nonlinearity [30,31]. With these specific mode combinations, some collinear and non-collinear wave mixing methods were developed to detect and locate different incipient damage in a plate such as fatigue [32], thermal degradation [30], and micro-cracks [33]. However, most existing wave mixing techniques use quadratic nonlinearity so that their sensitivity to incipient damage is relatively low compared with those techniques based on cubic nonlinearity. Relevant to the cubic nonlinearity-related wave mixing, Liu et al. proposed a general theoretical framework to analyze the cubic wave field induced by the mixing of two primary waves [21]. However, only analytical analyses were provided in that work. Sampath and Sohn proposed a three-wave mixing technique by introducing three primary Lamb waves to the nonlinear waveguide and detecting the combinational cubic wave components [34]. With the mode combination that satisfies the non-zero power flux and phase matching conditions, the cubic nonlinearity was successfully applied to detect fatigue cracks in a metal plate [35]. Nevertheless, it goes without saying that the use of three independent wave excitation channels inevitably increases the complexity of the physical system.

Apart from the aforementioned nonlinearities, a nonlinear cross-modulation/modulation transfer phenomenon was observed in elastic waves by Zaitsev et al. [36]. By emitting a single-frequency probe longitudinal wave (f_1) and a modulated pump longitudinal wave ($f_{2,2\pm m}$) through two physical channels in a rod with cracks, the single-frequency wave was modulated with the modulation frequency of the modulated wave as illustrated in Fig. 1. In a series of their following work, Zaitsev et al. demonstrated that the

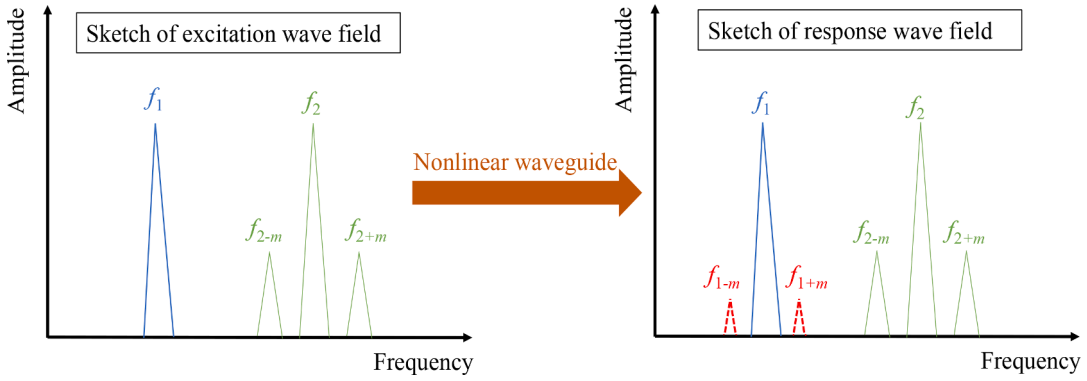

Fig. 1. Illustration of the cross-modulation phenomenon.

cross-modulation was induced by the cubic nonlinearity, which could be used to detect micro-scale cracks with higher sensitivity than conventional modulation technique based on quadratic nonlinearity [37–39]. It was found that the observed cross-modulation phenomenon was induced by the non-classical nonlinear wave dissipation at the crack, which resembles the so-called Luxemburg-Gorky (L-G) effect in radio waves [40–43]. Therefore, the observed cross-modulation in elastic waves was also referred to as L-G effect in their work. In the context of guided waves, Aymerich and Staszewski experimentally measured the cross-modulation of the Lamb waves and detected the impact damage in a composite plate [44]. However, all these existing studies on cross-modulation fall under the umbrella of vibroacoustic modulation where the modulated pump wave is excited with a continuous signal. This makes it less flexible for NDE applications than the wave mixing technique where both waves can be flexibly tuned in both time and frequency domains. Most importantly, the nonlinear source in the aforementioned existing works is the crack-type defect. Whether similar phenomena can be observed in a weakly nonlinear guided medium, and if so, how they are related to the well-known L-G effect remain an intriguing problem to be tackled. This motivated the present work.

More specifically, this work attempts to address the following questions which constitute its novelty:

- Can we observe the cross-modulation phenomenon in guided waves subjecting to wave mixing in a plate with material nonlinearity?
- If yes, what are the characteristics of the cross-modulated components (CMCs) generation in the context of guided waves?
- What are the potential advantages of guided wave cross-modulation for NDE applications?
- How does the cross-modulation phenomenon in guided waves relate to the L-G effect?

Targeting these questions, this work starts from a theoretical analysis on the characteristics of the CMC generation by considering different wave mixing patterns between single-frequency and modulated waves in a weakly nonlinear plate in Section 2. Finite element simulations are then conducted to confirm the characteristics of CMCs in Section 3. Specifically, a codirectional SH0 wave mixing scheme is highlighted which allows the generation of internally-resonant CMCs at all frequencies. The underlying mechanisms of the CMCs associated with the SH0 waves are further explored to illustrate the superiority of the CMCs for NDE applications. Section 4 presents experimental evidence on the measured CMCs in an aluminum plate subjecting to the codirectional SH0 wave mixing scheme. The relevance of the observed CMCs to the L-G effect is then discussed in Section 5, leading to the Conclusions summarized in Section 6.

2. Theoretical analyses on guided wave cross-modulation

We examine the cross-modulation of guided waves in the context of wave mixing in a plate with weak material nonlinearity. A general theoretical framework on wave mixing considering both quadratic and cubic nonlinearities is proposed, followed by the analyses on the characteristics of the CMCs generation in guided waves.

2.1. A general theoretical framework for wave mixing

Consider a pair of plane guided waves (a single-frequency wave indicated by subscript 1 and a modulated wave by subscript 2, $2\pm m$ as illustrated in Fig. 1) propagating in a weakly nonlinear plate along X direction with displacement u expressed as

$$\mathrm{u}_1(X,Y) = A_1\mathrm{U}_1(Y)\mathrm{e}^{\mathrm{i}(k_1X-\omega_1 t)} + c.c. \tag{1}$$

$$\begin{aligned}\mathbf{u}_{2,2\pm m}(X,Y) &= A_2\mathbf{U}_2(Y)\mathrm{e}^{\mathrm{i}(k_2X-\omega_2 t)} + A_{2+m}\mathbf{U}_{2+m}(Y)\mathrm{e}^{\mathrm{i}(k_{2+m}X-(\omega_2+\omega_m)t)}\\ &+A_{2-m}\mathbf{U}_{2-m}(Y)\mathrm{e}^{\mathrm{i}(k_{2-m}X-(\omega_2-\omega_m)t)} + \mathrm{c.c.}\end{aligned} \tag{2}$$

where Y is the thickness-wise direction. The amplitude and wave structure (normalized displacement distribution across the plate thickness) of a specific guided wave mode, either Lamb wave or SH wave, are denoted as A and U respectively. The wave number k and angular frequency ω of the wave are assumed to be positive. As such, Eqs. (1) and (2) describe the codirectionally propagating case of the single-frequency and modulated waves. The modulation frequency of the modulated wave is denoted by ω_m. The term c.c. stands for the abbreviated complex conjugate.

The stress-strain relation of the nonlinear elastic material is characterized with the Landau-Lifshitz model considering both quadratic and cubic nonlinearities as,

$$\begin{aligned}\mathbf{T}^{\mathbf{RR}} &= \lambda\mathrm{tr}[\mathbf{E}]\mathbf{I} + 2\mu\mathbf{E} + \overline{A}\mathbf{E}^2 + \overline{B}\mathrm{tr}\left[\mathbf{E}^2\right]\mathbf{I} + 2\overline{B}\mathrm{tr}[\mathbf{E}]\mathbf{E} + \overline{C}(\mathrm{tr}[\mathbf{E}])^2\mathbf{I} + \overline{E}\mathrm{tr}\left[\mathbf{E}^3\right]\mathbf{I}\\ &+3\overline{E}\mathrm{tr}[\mathbf{E}]\mathbf{E}^2 + 2\overline{F}\mathrm{tr}[\mathbf{E}]\mathrm{tr}\left[\mathbf{E}^2\right]\mathbf{I} + 2\overline{F}(\mathrm{tr}[\mathbf{E}])^2\ \mathbf{E} + 4\overline{G}\mathrm{tr}\left[\mathbf{E}^2\right]\mathbf{E} + 4\overline{H}(\mathrm{tr}[\mathbf{E}])^3\mathbf{I}\end{aligned} \tag{3}$$

where λ and μ are Lamé constants. The Landau third-order and fourth-order elastic constants are characterized by $\overline{A}$, $\overline{B}$, $\overline{C}$ and $\overline{E}$, $\overline{F}$, $\overline{G}$, $\overline{H}$ respectively (i.e., TOECs and FOECs). The tensor I is the second rank identity tensor and operation tr[] represents the trace. The second Piola-Kirchhoff stress tensor is denoted by T^{RR}. The Lagrangian strain tensor E is defined in terms of the displacement gradient, $H=\nabla$u, as

$$E = \frac{1}{2}\left(\mathrm{H} + \mathrm{H}^T + \mathrm{H}^T\mathrm{H}\right) \tag{4}$$

As the nonlinear wave components are much smaller than the primary waves in a weakly nonlinear elastic plate, the perturbation

theory is applied to decouple the system into linear and nonlinear parts. In addition, the governing equations for wave generation problems are more naturally written with the first Piola-Kirchhoff stress tensor S which relates to the second Piola-Kirchhoff stress tensor through the deformation gradient (I+H). Correspondingly, the stresses can be decomposed into linear, quadratic, and cubic terms as,

$$S = \mathrm{S^L} + \mathrm{S^Q} + \mathrm{S^C} = (\mathrm{I} + \mathrm{H})\mathrm{T^{RR}} \tag{5}$$

Detailed expressions of three terms are described in [21].

The mutual interaction between the single-frequency and modulated waves in the nonlinear plate entails nonlinear waves. Through combining the complex reciprocity theory and normal mode expansion method [21], the resultant nonlinear wave amplitude A_n for a designated wave mode n can be formulated as

$$4P_{nn}\left(\frac{\mathrm{d}}{\mathrm{d}X} - ik_n^*\right)A_n = f_n^{\mathrm{NL}}\mathrm{e}^{\mathrm{i}\left(\sum_{l=1}^{4} N_l k_{a_l}\right)X} \tag{6}$$

Where

$$f_n^{\mathrm{NL}} = -\mathbf{S^{NL}}(a_1, a_2, \ldots, a_l)\mathbf{V}_{\boldsymbol{n}}^*(Y)\cdot\mathbf{n}_Y\big|_{-h}^{h} + \int_{-h}^{h}\mathrm{Div}\left[\mathbf{S^{NL}}(a_1, a_2, \ldots, a_l)\right]\cdot\mathbf{V}_{\boldsymbol{n}}^*(Y)\,dY \tag{7}$$

$$P_{nn} = -\frac{1}{4}\int_{-h}^{h}\left(\mathrm{S}_n(Y)\mathrm{V}_n^*(Y) + \mathrm{V}_n(Y)\mathrm{S}_n^*(Y)\right)\cdot\mathrm{n}_X\,dY \tag{8}$$

$$N_l = 0,\ 1,\ 2\ldots,\ \sum_{l=1}^{4} N_l = q \tag{9}$$

In the above equations, a_l represent the four different frequencies of waves in the single-frequency and modulated waves in Eqs. (1) and (2). N_l are integers and their summation should be equal to the nonlinear order q which is either 2 or 3 in the present case. $f_n^{\mathrm{NL}}$is the nonlinear driving force term where the nonlinear driving stress $\mathrm{S^{NL}}$is obtained by substituting $(\mathrm{u}_1 + \mathrm{u}_{2,2\pm m})$ into Eq. (5). The quadratic and cubic terms can be separately extracted to further calculate the quadratic and cubic nonlinear wave fields. $\mathrm{V_n}$ and $\mathrm{S_n}$ stand for the normalized velocity and stress distributions across the plate thickness (from -h to h in the Y direction) of the nonlinear wave mode n. Superscript * denotes the complex conjugate. n_X and n_Y are the unit direction vectors along X (wave propagation direction) and Y (plate thickness direction) axis respectively. Finally, the nonlinear wave amplitude generated due to the mixing of the single-frequency and modulated waves can be calculated as

$$A_n(X) = \begin{cases} -\dfrac{\mathrm{i}f_n^{NL}}{4P_{nn}\left(k_n^* - \left(\sum_{l=1}^{4} N_l k_{a_l}\right)\right)}\left(\mathrm{e}^{\mathrm{i}k_n^* X} - \mathrm{e}^{\mathrm{i}\left(\sum_{l=1}^{4} N_l k_{a_l}\right)X}\right) & \text{if } k_n^* \neq \sum_{l=1}^{4} N_l k_{a_l} \\ \dfrac{f_n^{NL}}{4P_{nn}} X\mathrm{e}^{\mathrm{i}\left(\sum_{l=1}^{4} N_l k_{a_l}\right)X} & \text{if } k_n^* = \sum_{l=1}^{4} N_l k_{a_l} \end{cases} \tag{10}$$

Eq. (10) indicates that the internal resonance happens when the wavenumber of the generated nonlinear wave components matches with the combination of the wavenumbers of the single-frequency and modulated waves and the power flux from the single-frequency-modulated wave combination to the nonlinear wave is nonzero ($f_{\boldsymbol{n}}^{\mathbf{NL}} \neq 0$). In this case, the amplitude of the generated nonlinear waves will be linearly cumulative with respect to the wave propagating distance, which results in the large amplitude of nonlinear waves for ease of measurement in NDE applications.

2.2. Characteristics of cross-modulated component generation in guided waves

After deriving the nonlinear waves generated by the mixing of the modulated wave and single-frequency wave, the CMCs are investigated based on Eq. (10). To start, the quadratic nonlinearity is first evaluated by setting the value of q to 2. In this case, irrespective of the wave types of the single-frequency and modulated waves, Lamb waves or SH waves, codirectionally or counter propagating, the frequencies of nonlinear waves induced by wave mixing are limited to $\boldsymbol{\omega}_1 \pm \boldsymbol{\omega}_2$, $\boldsymbol{\omega}_1 \pm \boldsymbol{\omega}_2 \pm \boldsymbol{\omega}_m$, $\boldsymbol{\omega}_m$ and their conjugate counterparts. All possible combinations in the driving force terms are detailed in Appendix. It can be seen that cross-modulation cannot occur when only considering the quadratic nonlinearity.

Considering the cubic nonlinearity by setting the nonlinear order q to 3, various combinations of single-frequency and modulated wave combinations are formed as shown in Appendix. Specifically, the CMCs can be formed at $\boldsymbol{\omega}_1 \pm \boldsymbol{\omega}_m$. However, the nonlinear driving force terms are different, which depends on whether the single-frequency and the modulated waves are codirectional or counter directional. This leads to the following scenarios.

- For the codirectional mixing case, the CMCs-related nonlinear forcing terms include $e^{i((k_2-k_{2-m}+k_1)X-(\omega_m+\omega_1)t)}$, $e^{i((-k_2+k_{2-m}+k_1)X-(-\omega_m+\omega_1)t)}$, $e^{i((k_2-k_{2+m}+k_1)X-(-\omega_m+\omega_1)t)}$, $e^{i((-k_2+k_{2+m}+k_1)X-(\omega_m+\omega_1)t)}$ and their complex conjugate counterparts. In this case, when the single-frequency and modulated waves are SH0 waves, the generated CMCs should only be SH0 waves according to the power flux analyses. Meanwhile, benefiting from the non-dispersive nature of the SH0 waves, the wavenumber of the expected SH0 wave at the targeted frequency $\omega_1 \pm \omega_m$ automatically matches with that of the single-frequency-modulated wave combination. This means the generated CMCs will be cumulative at all frequencies. By comparison, if the single-frequency and modulated waves are Lamb waves, the CMCs can only be Lamb waves. However, due to the dispersive nature, only limited mode combinations can satisfy the phase matching condition.
- For the counter mixing case, the CMCs-related nonlinear forcing terms encompass $e^{i((k_2-k_{2-m}-k_1)X-(\omega_m+\omega_1)t)}$, $e^{i((-k_2+k_{2-m}-k_1)X-(-\omega_m+\omega_1)t)}$, $e^{i((k_2-k_{2+m}-k_1)X-(-\omega_m+\omega_1)t)}$, $e^{i((-k_2+k_{2+m}-k_1)X-(\omega_m+\omega_1)t)}$ and their complex conjugate counterparts. In this case, no matter the single-frequency and modulated waves are Lamb waves or SH waves, only limited mode combinations can satisfy the phase matching condition. Specifically, for the non-dispersive SH0 wave combinations, no frequency combinations can satisfy this condition.

To sum up, this analysis shows that CMCs through guided wave mixing only correspond to the cubic nonlinearity instead of the quadratic nonlinearity in a weakly nonlinear guided medium. In addition, a codirectional SH0 wave mixing scheme features cumulative properties of the CMCs with arbitrary frequency combinations.

3. Numerical studies: validations and mechanism explorations

3.1. Model description

Numerical simulations are then carried out to verify the characteristics of CMCs in guided waves and further explore the underlying physical mechanisms. To this end, a three-dimensional finite element model is established on a 300mm-long (X direction) and 1mm-thick (Y direction) aluminum plate in Abaqus/Explicit as shown in Fig. 2. The width (Z direction) of the plate is 0.15mm with a periodic boundary condition imposed to ensure plane guided waves in the plate. SH waves and Lamb waves are generated using the prescribed displacements at the end of the plate. The single-frequency and modulated signals are both tone-burst signals with the same duration of 40 μs. Their respective central frequencies are arbitrarily selected as 500kHz and 1200kHz, respectively with a sampling frequency of 100MHz. The frequency of the modulated signal is set to 125kHz. The mesh size is 0.05mm which ensures around 20 elements per smallest wavelength under consideration. The mass density of the aluminum is 2700kg/m^3 and the elastic constants are listed in Table 1. It is worth noting the material nonlinear behavior is introduced to the finite element model via a user material subroutine (VUMAT in Abaqus).

3.2. Confirmation of the cross-modulated component generation

The case of codirectional mixing of SH0 waves is first investigated. A prescribed displacement in the Z direction is applied at the left end of the plate for both single-frequency and modulated wave excitations. The amplitude of both waves is set to 1μm. Displacement in the Z direction (U3) is used to characterize the SH wave response. Specifically, a subtraction method [32] is used to extract the nonlinear wave field due to wave mixing as illustrated in Fig. 3. First, both single-frequency and modulated waves are excited in the plate and T(1+2) denotes the response at 140mm to the left end in Fig. 3(a). After that, the modulated and single-frequency waves are separately excited in the plate and their respective responses, T(1) and T(2), are shown in Figs. 3(b) and (c), respectively. Through the subtraction, the nonlinear wave can be extracted in the time domain in Fig. 3(d) as $T(1+2)-T(1)-T(2)$. The spectra of the received signals are then analyzed with the Fast Fourier transform (FFT). Fig. 4(a) shows the spectra of the overall response in Fig. 3(a) where the frequency components of the primary waves are dominant. Fig. 4(b) shows the spectra of the extracted nonlinear response in Fig. 3(d). Various frequency components can be observed corresponding to different combinations of the single-frequency and modulated waves in Fig. 4(b). Specifically, the sidebands of the single-frequency wave appear at f_{1-m} (375kHz) and f_{1+m} (625kHz), which correspond exactly to the cross-modulation phenomenon predicted by the theoretical model. This demonstrates that the CMCs are

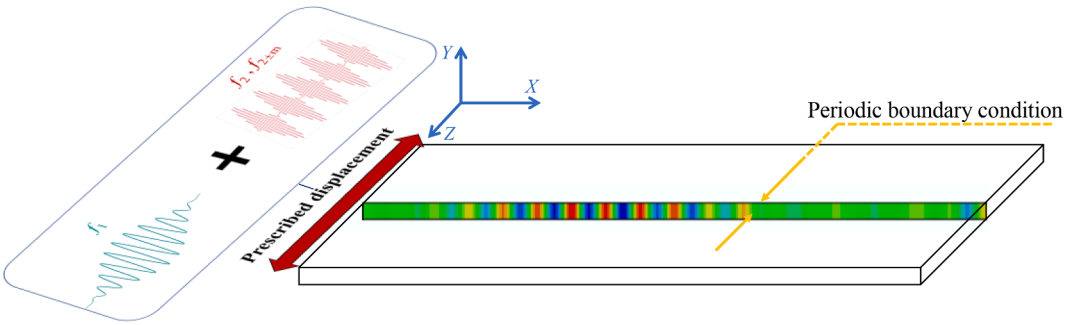

Fig. 2. The finite element model.

Table 1
Elastic constants of aluminum. (Unit: GPa).

λ	μ	$\overline{A}$	$\overline{B}$	$\overline{C}$	$\overline{E}$	$\overline{F}$	$\overline{G}$	$\overline{H}$
55.27	25.95	−351.2	−140.4	−102.8	400	−406	347	72

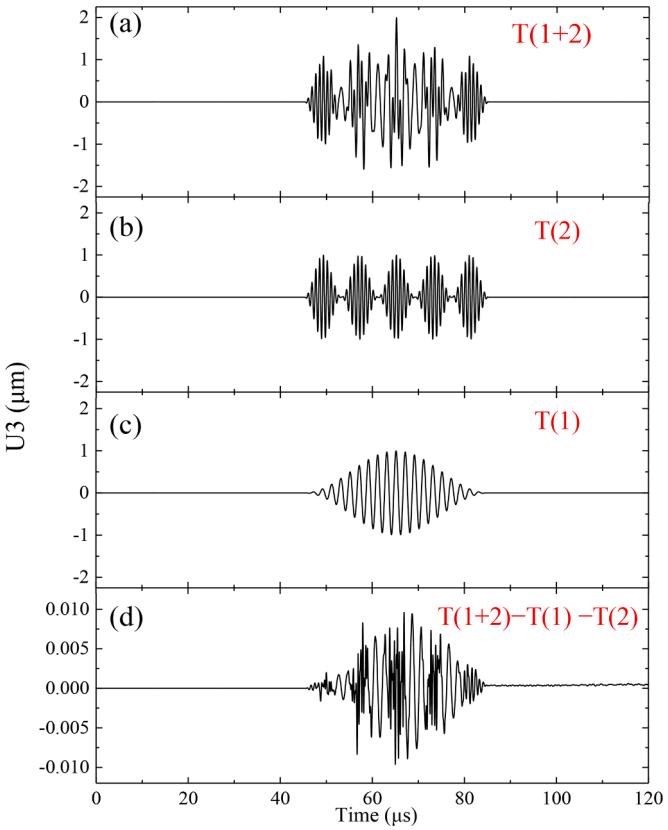

Fig. 3. Received signals for at a point 140mm away from the excitation: (a) when both the single-frequency and modulated waves are excited; (b) when only the modulated wave is excited; (c) when only the single-frequency wave is excited; (d) the extracted nonlinear signal.

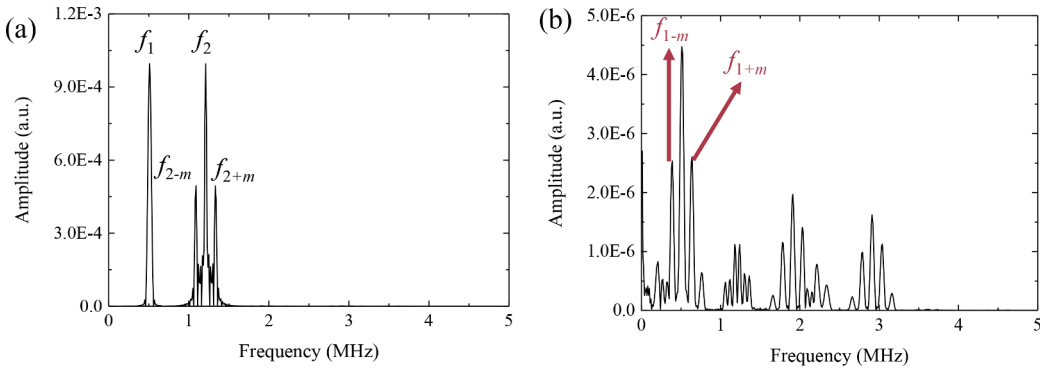

Fig. 4. Spectra of the responses: (a) T(1+2); (b) T(1+2)−*T*(1)−*T*(2).

effectively generated by the codirectional SH0 wave mixing. In addition, the responses corresponding to different wave propagating distances are extracted to assess the cumulative effect. Specifically, three typical extracted nonlinear responses corresponding to the propagating distances of 100mm, 140mm, and 180mm are examined in Fig. 5. The increase of the nonlinear wave amplitude with respect to the increasing wave propagating distance in both time-domain (Fig. 5(a)) and frequency-domain (Fig. 5(b)) signals clearly

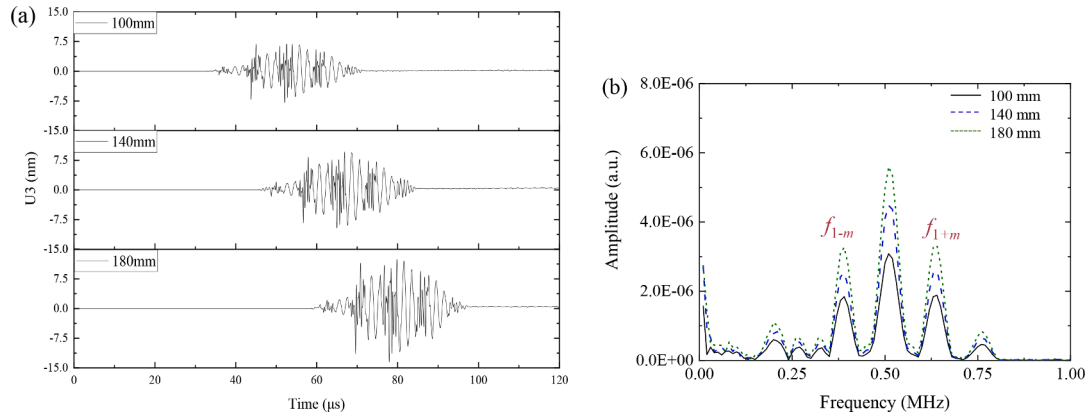

Fig. 5. The extracted nonlinear SH wave responses at different wave propagating distances: (a) time-domain signals and (b) their spectra.

demonstrate the cumulative feature of the CMCs as predicted by the theoretical analyses.

Then, other mixing patterns are studied to evaluate their influence on the CMCs generation considering different wave mixing directions and different primary wave modes as shown in Fig. 6. Specifically, the case of counter mixing of SH0 waves is first studied. The single-frequency and modulated waves are generated at the two ends of the plate. Other settings in the finite element simulation are identical to the above codirectional mixing case. With the subtraction method, the nonlinear response at 140mm from the left end is extracted and the spectrum is calculated as shown in Fig. 6(a). The sidebands corresponding to the CMCs cannot be observed.

The codirectional and counter mixing of Lamb waves cases are then studied. The prescribed displacement in the *X* direction (U1) is uniformly applied at the ends for both single-frequency and modulated waves excitation and the corresponding U1 on the top surface is calculated to quantify the Lamb wave responses. The amplitudes of the two waves are set to 0.1μm to ensure the convergence of calculation. The frequencies of the two waves are identical to the previous cases so that S0-mode Lamb waves are generated. For both codirectional and counter mixing cases of Lamb waves, the arbitrarily chosen frequency combination does not satisfy the phase matching condition according to the theoretical analyses. The codirectional Lamb wave mixing case is first studied. The nonlinear response at 140mm from the left end and its spectrum are extracted and shown in Fig. 6(b). Although some combinational frequencies appear in the spectrum, they are associated with the quadratic nonlinearity resulting from the calculation. The CMCs induced by the cubic nonlinearity are suppressed and therefore cannot be observed. Following the same procedure, the CMCs in the counter mixing of Lamb waves case do not appear either as shown in Fig. 6(c). These observed phenomena agree well with the theoretical predictions.

Remarkably, through scrutinizing different guided wave mixing patterns, it is demonstrated that the CMCs can be flexibly generated in the codirectional SH0 wave mixing scheme irrespective of frequency combinations. In addition, the cumulative effect of CMCs predicted by the theoretical analysis is validated, which is of great benefit for further NDE applications.

3.3. Mechanisms of the cross-modulated component generation and their advantages for damage detection

After demonstrating the cumulative CMCs in the codirectional SH0 mixing scheme, the underlying mechanisms are further investigated and their advantages for incipient damage detection in NDE applications are discussed in this section.

Following the previous work in [22], it can be surmised that there are two generation mechanisms of CMCs to get the pure and mixed CMCs respectively. As shown in Fig. 7, the former is directly due to the FOECs while the latter is a result of the mixing of the primary waves and their generated secondary combinational harmonics through TOECs. To verify this, the TOECs and FOECs are separately introduced into the finite element model in the codirectional SH0 wave mixing case. First, with only the TOECs, the extracted nonlinear response at 140mm from the left end is extracted and denoted as S_{TOEC}. The TOECs are then multiplied by a factor of 2 and the corresponding nonlinear response at the same position is defined as $S_{2\times TOEC}$. According to the mixed CMC generation mechanism, the doubling of the TOECs should result in quadruple CMCs. Therefore, the S_{TOEC} is multiplied by a factor of 4 and compared with $S_{2\times TOEC}$ as shown in Figs. 8(a) and (b). It can be seen the amplitudes of the two signals match well for the CMCs. Similarly, for the validation of the pure CMCs generation mechanism, only FOECs are included in the simulations. The nonlinear responses before and after the FOECs are doubled are marked as S_{FOEC} and $S_{2\times FOEC}$ respectively. The comparison is made by the double of S_{FOEC} and $S_{2\times FOEC}$ as presented in Figs. 8(c) and (d). It can be seen the CMCs in the two signals also perfectly match. Therefore, the two mechanisms of the CMCs generation are confirmed. It is worth noting that the mixed CMCs are waveringly cumulative due to the phase velocity mismatch between the primary SH0 waves and the secondary Lamb waves according to [22]. Since the internal resonance between the primary waves and tertiary waves is dominant, the wavering feature is very weak and the mixed CMCs still retain the cumulative effect.

The potential of the CMCs for incipient damage detection is further discussed based on the aforementioned generation mechanisms. Specifically, a previously developed two-SH-wave-mixing technique based on quadratic nonlinearity is used for comparison [32]. In that method, the generated nonlinear Lamb waves are used to characterize material property changes related to incipient damage. By using the same model as the codirectional mixing of SH0 wave case in this work, the out-of-plane displacement at 140mm from the left

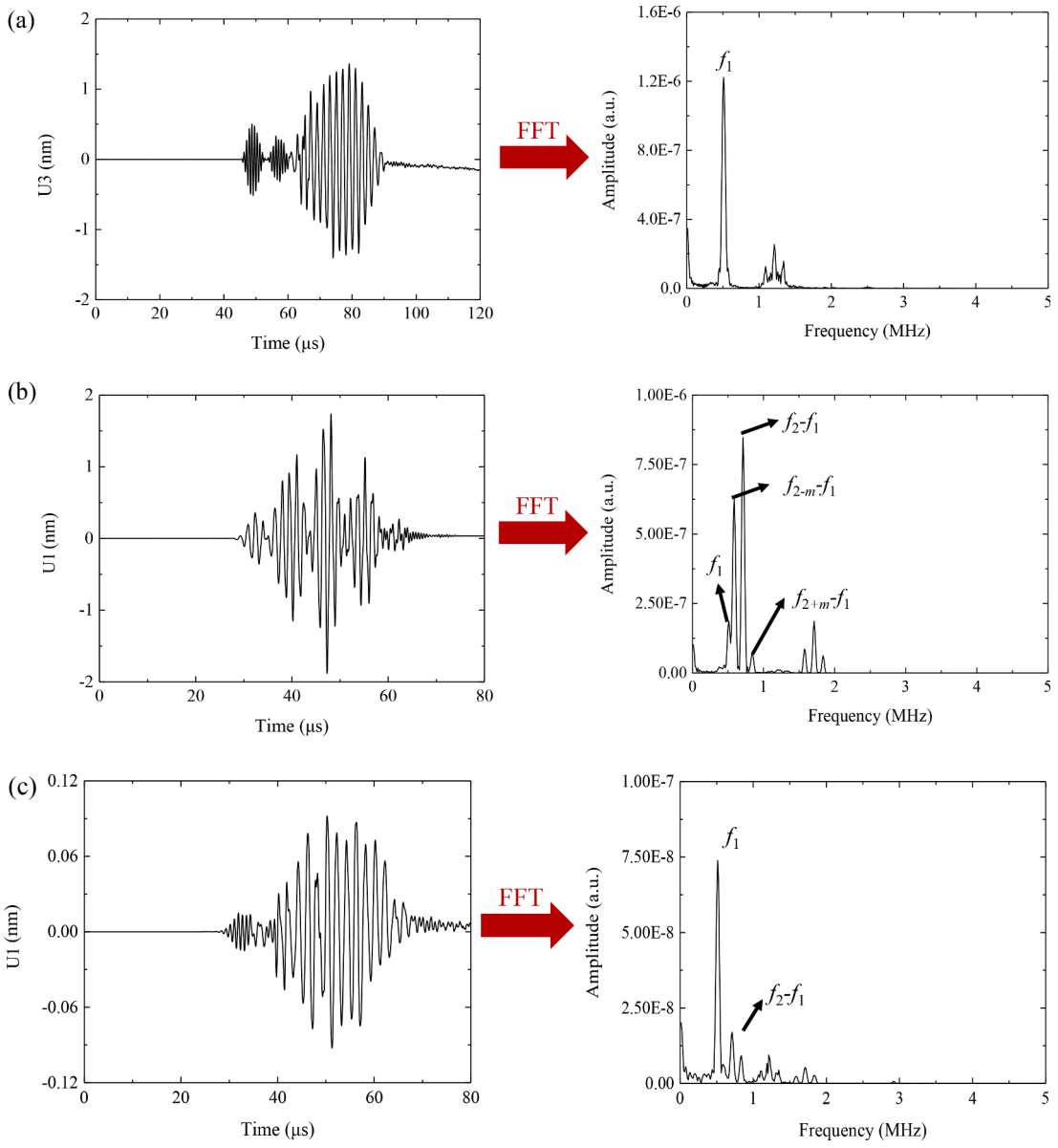

Fig. 6. (a) Nonlinear SH wave response in the counter SH0 wave mixing case; (b) nonlinear Lamb wave response in the codirectionally S0 wave mixing case; (c) nonlinear Lamb wave response in the counter S0 wave mixing case.

end is extracted to characterize the nonlinear Lamb waves. When the TOECs are doubled, the nonlinear response at the combinational frequencies also doubles, as evidenced in Fig. 9. Compared with the results in Figs. 8(a) and (b), it is evident that CMCs present higher sensitivity than the two-SH-wave-mixing technique subjecting to the same degree of changes in the TOECs. In addition, according to the literature [34,45], when the structure is subjected to material degradation, the change of the FOECs is much larger than that of the TOECs, which further contributes to the higher sensitivity of the CMCs. Besides, as the generation of CMCs requires the mixing of two waves, the complexity of the physical system will not be increased and the immunity to the deceptive nonlinearities from the measurement system instruments can still be preserved.

4. Experimental confirmation

Experiments are conducted to first confirm the CMCs in the codirectional SH wave mixing case and then discuss their relevance to the L-G effect. The experimental setup is illustrated in Fig. 10. A 700mm × 500mm × 2mm aluminum (2A12 alloy) plate is tested with three magnetostrictive transducers (MsTs) installed at positions sketched in Fig. 10(b). Typically, an MsT contains a magnetostrictive element which is the iron-cobalt foil (70mm × 50mm × 0.2mm) in this case, a coil to generate the dynamic magnetic field and a

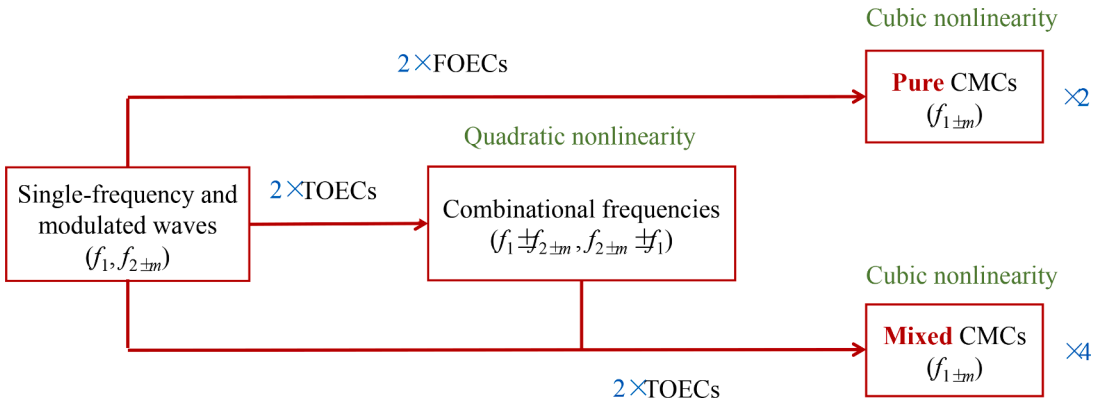

Fig. 7. Mechanism of the cross-modulated components (CMCs) generation subjecting to the codirectional SH0 wave mixing scheme.

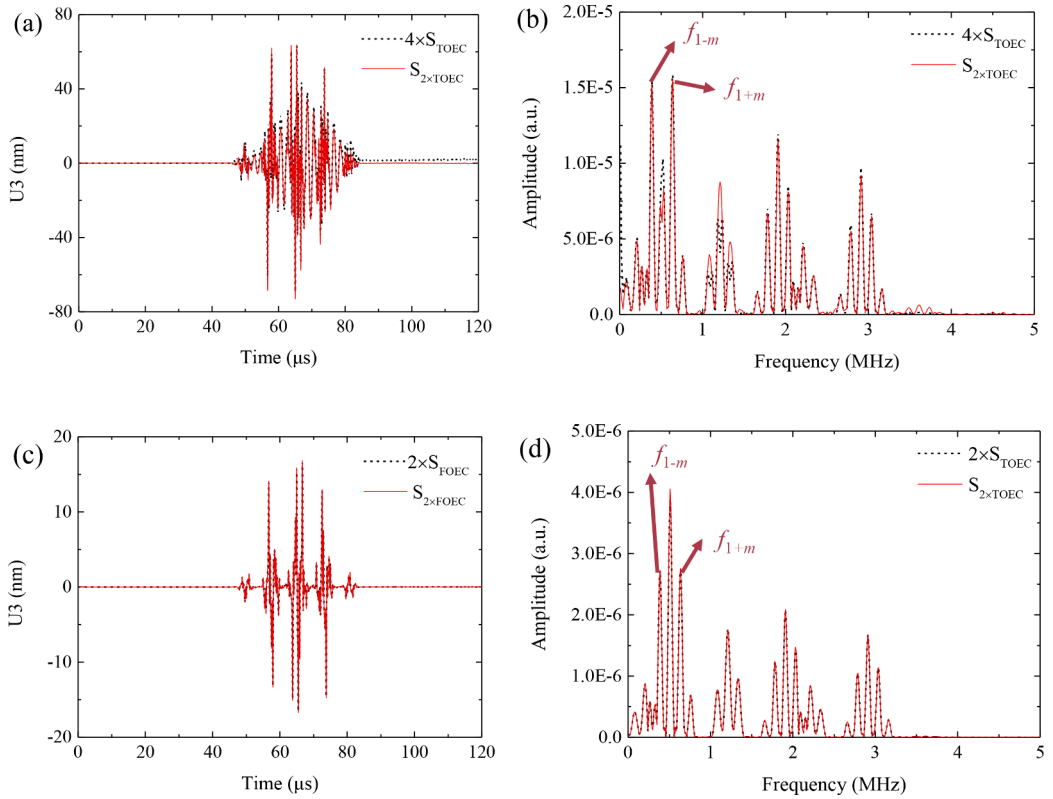

Fig. 8. (a) and (b) time-domain responses of the mixed CMCs and their spectra; (c) and (d) time-domain responses of the pure CMCs and their spectra.

permanent magnet to provide the static bias field [46]. When the static and dynamic magnetic fields are perpendicular, SH waves can be effectively generated and received. Specifically, the spacing of the coil can be tuned to match the wavelength/frequency of the targeted SH waves. The measurement system works as follows. A KEYSIGHT® 33500B waveform generator outputs two signals corresponding to the single-frequency and modulated waves which are amplified by two RITEC® GA-2500A power amplifiers. The amplified signals then feed the two MsT actuators for SH wave generation. The two actuators are slightly misaligned to ensure the approximate codirectional wave mixing considering the wave beam divergence effect. This guarantees that the wave mixing only takes place in the plate to avoid any nonlinear interference from the measurement system. The generated SH waves propagate in the plate and are further captured by the MsT sensor. The response signal is recorded with the National Instruments® PXIe 5105 Oscilloscope.

In the experiment, the central frequency of the single-frequency wave is set to 200kHz which is sent to the coil with 15.5mm spacing. The modulated wave is centered at 300kHz with the modulation frequency of 30kHz in Fig. 11 which is applied to the coil with a spacing of 10.3mm. The duration of both the single-frequency and modulated signal is 100 μs. Both excitation signals are

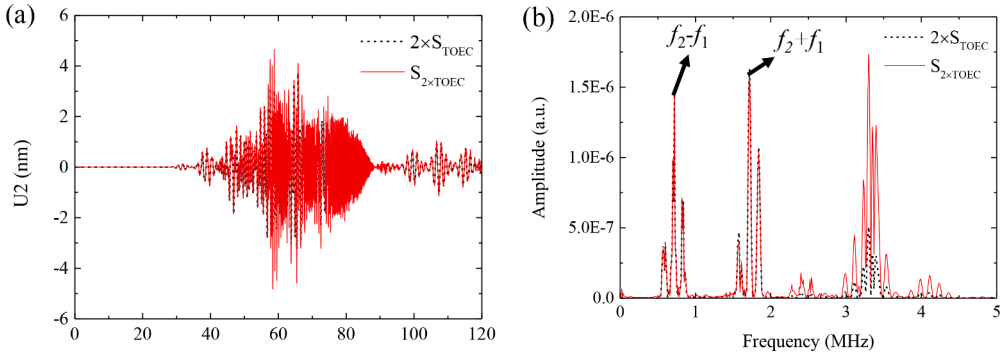

Fig. 9. Influence of material parameter change on the nonlinear wave generation in the two-wave mixing technique with quadratic nonlinearity: (a) time-domain responses and (b) spectra.

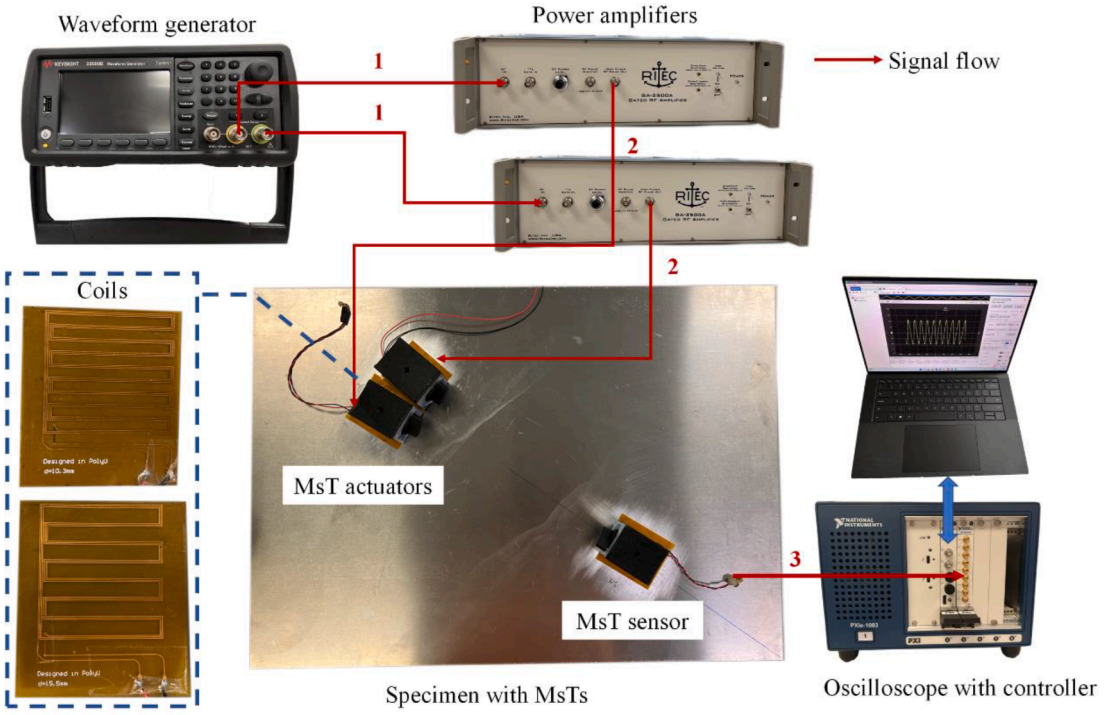

Fig. 10. The experimental setup.

amplified to 900V by the power amplifier and applied to the MsTs. The spacing of the coil at the sensing unit is selected as 15.5mm. The sampling frequency of the oscilloscope is 10MHz.

Following the principle of the subtraction method, the single-frequency and modulated waves are simultaneously excited first and then activated separately. The response signals as well as their difference are obtained and shown in Fig. 12. Apart from the electromagnetic crosstalk, the first arrivals in the response signals can be clearly separated from the boundary reflections. The wave packets corresponding to the first arrivals can be identified as SH0 waves as judged by the wave propagation speed. It is observed that the amplitude of the extracted nonlinear wave signal ($T(1+2)-T(1)-T(2)$) is less than 1% of the overall response ($T(1+2)$), which indicates the weak nonlinearity of the plate. After that, the FFT is applied to windowed wave packets in the overall response and extracted nonlinear signal in Fig. 12 alongside the corresponding spectra are obtained in Fig. 13. Similar to the numerical results, the overall response mainly contains the dominant frequency components of the single-frequency and modulated waves while the CMCs can be observed in the extracted nonlinear signal. As the wave mixing only takes place in the plate, the measured CMCs should only attribute to the material nonlinearity of the plate. Since material nonlinearity is usually induced by material microstructure defects [19], the CMCs hold great promise for further incipient damage detection applications.

The characteristics of the measured CMCs are further explored to evaluate their relevance to the L-G effect. As demonstrated in [36], the L-G effect applies to elastic waves resulting from the nonlinear wave dissipation which is evidenced by the decrease of the

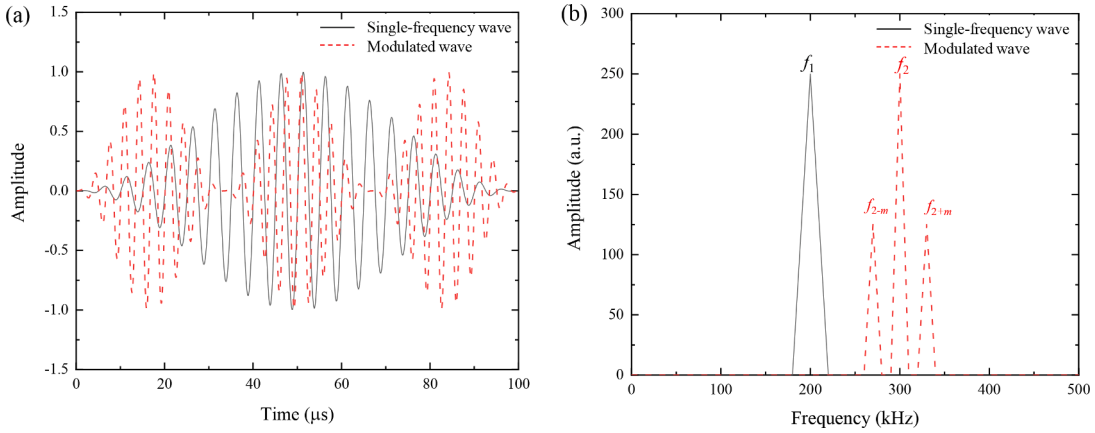

Fig. 11. (a) The normalized excitation signals of the single-frequency and modulated waves and (b) their spectra.

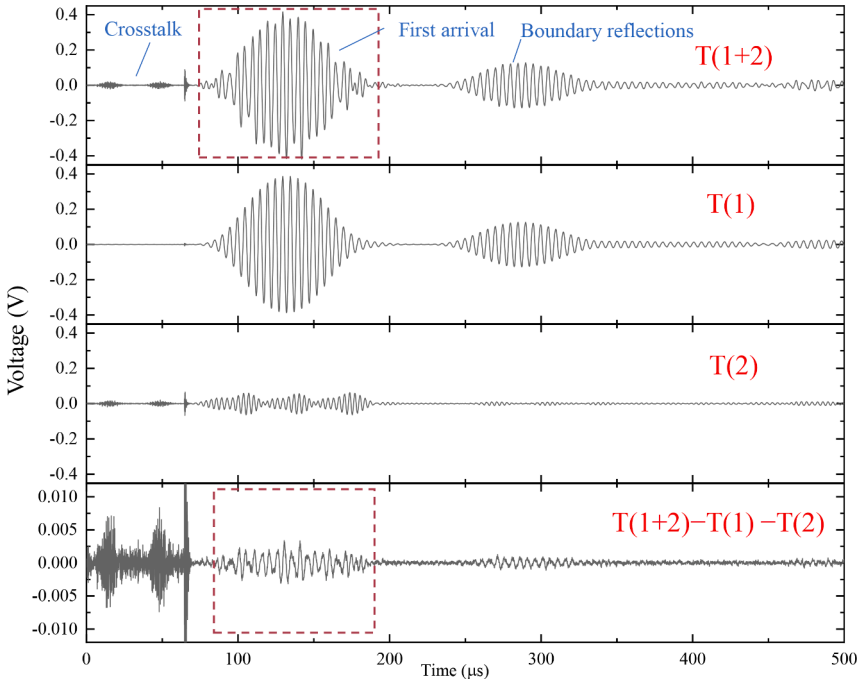

Fig. 12. The received time-domain responses of the MsT sensor following the procedure of the subtraction method.

single-frequency probe wave amplitude with the increase of the modulated pump wave amplitude. Following the same procedure, while the input voltage of the single-frequency wave is fixed at 900V, the amplitude of the modulated excitation signal is varied from 500V to 1100V with an incremental step of 100V. The amplitudes of both the single-frequency response and CMCs are extracted with the FFT as illustrated in Fig. 13 and the results are obtained in Fig. 14. Each test is repeated three times and the error bar is calculated to minimize the influence of system inconsistency. It can be seen that the amplitudes of the CMCs increase with respect to the modulated wave amplitude in Fig. 14(a). However, with the increase of the modulated wave, the variation of the amplitude of the single-frequency wave is less than 0.5%, which can be deemed almost unchanged in Fig. 14(b). Similarly, we then fix the input voltage of the modulated wave at 900V while changing the single-frequency excitation level from 500V to 1100V. Results in Fig. 15 show again that the cross-modulation phenomenon is enhanced with the increase of the single-frequency excitation (Fig. 15(a)). However, the amplitudes of the three frequency components in the modulated wave remain nearly constant with a maximum variation of 0.2%. These observations indicate that the mechanism of the CMCs generation in a weakly nonlinear plate is different from the nonlinear wave dissipation of the L-G effect.

To sum up, experiments confirm the existence of the CMCs arising from the codirectional SH0 wave mixing in a weakly nonlinear plate. Despite the similar cross-modulation phenomenon, the measured CMCs in guided waves are induced by the nonlinear elasticity,

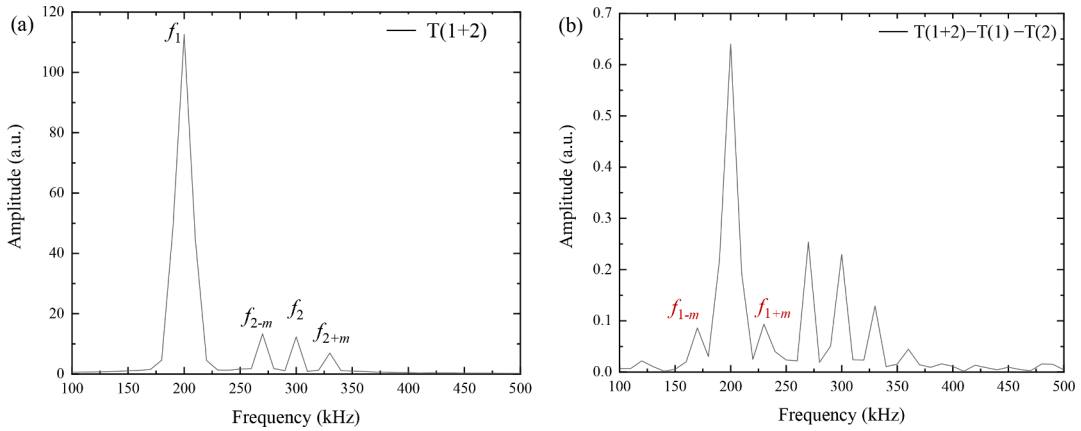

Fig. 13. Spectra of the windowed wave packets in the (a) overall response and (b) extracted nonlinear response.

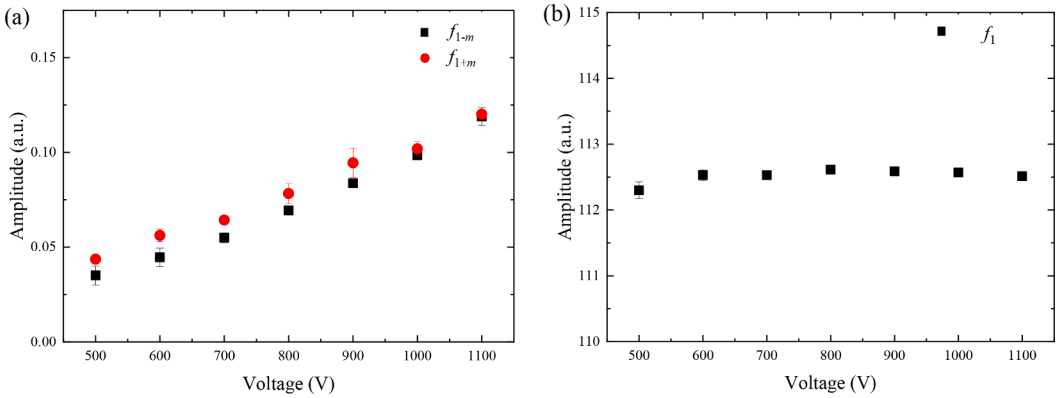

Fig. 14. Influence of the excitation amplitude of the modulated wave on the responses of the (a) CMCs amplitudes and (b) the modulated wave amplitudes.

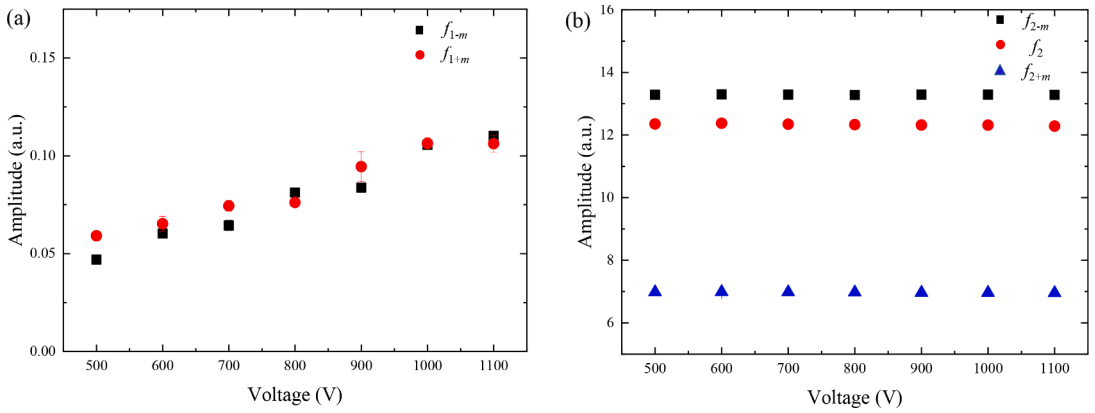

Fig. 15. Influence of the excitation amplitude of the single-frequency wave on the responses of (a) the CMCs amplitudes and (b) the modulated wave amplitudes.

instead of the nonlinear dissipation associated with the L-G effect.

5. The relevance of the cross-modulation phenomenon in guided waves to the Luxemburg-Gorky effect

By now, the cross-modulation of guided waves has been studied analytically, numerically, and experimentally. Since similar wave

Table 2
A summary of the characteristics of the original L-G effect in radio waves, the L-G effect retooled for elastic waves, and the cross-modulation for guided waves.

Cross-modulation effects	Wave cross-modulation - wave interaction in which the modulation of one wave is imposed nonlinearly on the other wave Known as the original Luxemburg-Gorky (L-G) effect	Known as the L-G effect retooled for elastic waves	Cross-modulation for ultrasonic guided waves
Type of wave	Electromagnetic waves (radio waves)	Mechanical waves (ultrasonic bulk waves)	Ultrasonic guided waves
Wave propagation medium	Lower ionosphere, plasma, liquid	Solids (glass, aluminum, CFRP)	Solids (aluminum)
Type of nonlinearity	Distributed and local (weakly ionized plasma, liquid with micro-bubbles)	Local (fatigue crack, delamination)	Distributed (weak material nonlinearity)
Nonlinear parameter	Dissipation (wave attenuation)	Non-classical (i.e., non—frictional, non-adhesion-hysteretic) dissipation	Elasticity
Physical explanation	Two theories used to explain the variation in the absorption of the medium: • The non-kinetic theory is based on the theory of the electric waves in the ionosphere; the absorption variation is caused by the modulation of plasma temperature due to heating, caused by the powerful propagating wave • The kinetic theory is based on the Boltzmann equation for electrons; the wave modulation leads to the modulation of the electron energy distribution	Physical explanation still not fully understood; no model provided but only some literature-based observations: • Nonlinear coupling between the strain and temperature fields • The role of inner contact in cracks and of thermo-elastic coupling in imperfect solids is underlined in the wave attenuation (local concentration of stress and temperature gradient) • Crack behavior similar to polycrystalline materials	The classical wave mixing theory used to explain the effect: • The cross- modulation due to cubic – rather than quadratic – nonlinearity • Two generation mechanisms of the modulation transfer, i.e., pure (through the FOECs) and mixed (the primary wave mixed with the secondary harmonics generated through the TOECs)
Observations and comments	• Amplitude modulation only transferred • Amplitude modulation predominantly picked up • Self-demodulation observed – i.e., modulation transfer acts to lessen the original modulation • The effect is enhanced if the fundamental frequency of either wave is close to the electron gyrofrequency	• Experimentally observed for low strain levels that are not sufficient to open the crack • Cross-modulation observed predominantly for the crack-tearing mode • Experimental evidence showing the link between the intensity of modulation and the local temperature field in the crack vicinity • Used for damage detection (crack detection in metals and impact damage detection in composites)	• No additional phase matching condition for the co-directional SH0 wave mixing to generate cumulative CMCs • For Lamb waves and counter propagating SH waves, only limited mode combinations can satisfy the phase matching leading to the cross- modulation • Better sensitivity to microstructural damage than the classical wave mixing method
Examples of references	[40–43]	[37,44]	_

propagation phenomena have been observed for different types of waves in physics, the question arises as to what degree the newly discovered mechanism reported in this work is related to previously investigated wave cross-modulations, in particular the L-G effect reported in the open literature.

The L-G effect is unquestionably one of the salient nonlinear wave interaction phenomena related to cross-modulation. The L-G effect has been observed originally for electromagnetic radio waves propagating in the lower ionosphere. The nonlinearity leading to the cross-modulation in radio waves can be either distributed or local nonlinearity, exemplified by the weakly ionized plasma and liquid with micro-bubbles, respectively. The cross-modulation observed in ultrasonic bulk wave propagation which is claimed to be the L-G effect retooled for elastic waves stems from the local nonlinearity associated with the crack-wave interaction. The cross-modulation mechanism for guided waves investigated in the paper, however, relates to the distributed weak material nonlinearity in a guided medium. Regarding the type of nonlinearity, both the cross-modulation for guided waves and the retooled L-G effect for the elastic waves resemble the original L-G effect for radio waves in different aspects. Specificities and comparisons among the three types of cross-modulations are summarized in Table 2.

In contrast to the original and retooled L-G effect, the cross-modulation for guided waves is induced by nonlinear elasticity rather than nonlinear dissipation. As to the retooled L-G effect, the nonlinear dissipation and non-classical physical behavior are probably the only two elements similar to the original L-G effect, which indicates why the cross-modulation observed for the crack-wave interaction in ultrasonic wave propagation has been claimed to be the L-G effect retooled for elastic waves. If nonlinear dissipation in cross-modulation characterizes uniquely the L-G effect, the investigated modulation transfer mechanism does not relate to it.

In summary, the question whether the investigated modulation transfer effect relates to the original L-G effect is still open. Although the theoretical model behind the nonlinear effect investigated has been proposed and validated numerically and experimentally, further research work is still required to answer this question.

6. Conclusions

This work investigates the cross-modulated component (CMC) generation in guided waves residing in a weakly nonlinear medium. Theoretical analyses are first carried out to ascertain the characteristics of the CMC generation subjecting to different wave mixing patterns. Finite element studies are then conducted to verify the theoretically predicted cross-modulation phenomena. The underlying mechanisms of the CMC generation in the codirectional SH0 wave mixing scheme are further investigated and the superiority of the CMCs for NDE applications is discussed. Experiments are conducted to confirm the generated CMCs in the codirectional SH0 wave mixing case. The relevance of the observed cross-modulation in guided waves to the original L-G effect in radio waves and the L-G effect retooled for elastic waves based on nonlinear dissipation is finally elucidated.

It is found that CMCs are generated because of the cubic nonlinearity instead of the quadratic nonlinearity. Specifically, a codirectional SH0 wave mixing scheme is highlighted which allows the generation of internal-resonant CMCs under arbitrary frequency combinations of single-frequency and modulated waves. In addition, pure and mixed CMCs generation mechanisms are identified which are separately related to the FOECs and TOECs. Although the material-nonlinearity-induced CMCs exhibit similar behavior as the crack-induced cross-modulation phenomenon reported in the literature, they stem from different mechanisms: i.e., nonlinear elasticity and nonlinear dissipation, respectively. Therefore, whether the material-nonlinearity-induced CMCs in guided waves can be termed the L-G effect remains an open question.

Nevertheless, the uncovered CMCs in guided waves induced by distributed material nonlinearity provide a new possibility for incipient damage detection in NDE applications before the initiation of crack-type defects. Compared with the conventional two-wave mixing techniques, CMCs exhibit higher sensitivity to incipient damage. In addition, by using two wave excitation channels, the complexity of the physical system is not increased but the advantage of being immune to instrumentation nonlinearity is still preserved. In addition, the flexible choice of frequency combinations in the codirectional SH0 wave mixing scheme offers enormous flexibility for practical applications.

In a broader sense, when the cross-modulation is used to detect localized defects (cracks), the distributed material nonlinearity acts as a masking/background nonlinearity. The influence of the masking nonlinearity on the detection of crack-type defects should be thoroughly evaluated. This points to the future direction to better understand and apply the L-G effect for NDE applications by considering both localized and distributed nonlinearity under the same roof.

Declaration of Competing Interest

The authors declare that they have no known competing financial interests or personal relationships that could have appeared to influence the work reported in this paper.

Data availability

Data will be made available on request.

Acknowledgments

The work was supported by grants from the Research Grants Council of Hong Kong Special Administrative Region (PolyU 152013/

21E), the National Natural Science Foundations of China through SHENG project (Polish-Chinese Funding Initiative, 51961135302, The Polish National Science centre grant nr UMO-2018/30/Q/ST8/00571), the Natural Science Foundation of Shanghai (22ZR1462700), the Fundamental Research Funds for the Central Universities and the Innovation and Technology Commission of the HKSAR Government to the Hong Kong Branch of National Rail Transit Electrification and Automation Engineering Technology Research Center. The authors would also like to thank Prof. Zhifeng Tang from Zhejiang University for kindly providing the iron-cobalt foils.

Appendix: Combinations of the wavenumber and frequency components in the nonlinear driving force terms

According to Eq. (10), the generated nonlinear waves due to the mutual interactions of the single-frequency and modulated waves are determined by the nonlinear driving force which is directly related to the nonlinear driving stress $\mathbf{S}^{\mathbf{NL}}$. For the codirectional mixing case, $\mathbf{S}^{\mathbf{NL}}$ is be obtained by substituting $(\mathbf{u}_1 + \mathbf{u}_{2,2\pm m})$ from Eqs. (1) and (2) into Eq. (5). The quadratic and cubic terms can be separately extracted according to the perturbation theory. Specifically, the terms related to quadratic nonlinearity include these combinations:

$$\mathbf{e}^{\mathbf{i}((k_2+k_1)X-(\omega_2+\omega_1)t)}, \mathbf{e}^{\mathbf{i}((k_2-k_1)X-(\omega_2-\omega_1)t)}, \mathbf{e}^{\mathbf{i}((k_{2+m}+k_1)X-(\omega_2+\omega_m+\omega_1)t)}, \mathbf{e}^{\mathbf{i}((k_{2+m}-k_1)X-(\omega_2+\omega_m-\omega_1)t)},$$

$$\mathbf{e}^{\mathbf{i}((k_{2-m}+k_1)X-(\omega_2-\omega_m+\omega_1)t)}, \mathbf{e}^{\mathbf{i}((k_{2-m}-k_1)X-(\omega_2-\omega_m-\omega_1)t)}, \mathbf{e}^{\mathbf{i}(-(k_2+k_1)X+(\omega_2+\omega_1)t)}, \mathbf{e}^{\mathbf{i}(-(k_2-k_1)X+(\omega_2-\omega_1)t)},$$

$$\mathbf{e}^{\mathbf{i}(-(k_{2+m}+k_1)X+(\omega_{2+m}+\omega_m+\omega_1)t)}, \mathbf{e}^{\mathbf{i}(-(k_{2+m}-k_1)X+(\omega_2+\omega_m-\omega_1)t)}, \mathbf{e}^{\mathbf{i}(-(k_{2-m}+k_1)X+(\omega_2-\omega_m+\omega_1)t)},$$

$$\mathbf{e}^{\mathbf{i}(-(k_{2-m}-k_1)X+(\omega_2-\omega_m-\omega_1)t)}.$$

The terms generated by the cubic nonlinearity have the following combinations with the terms corresponding to the CMCs underlined:

$$e^{i((2k_2+k_1)X-(2\omega_2+\omega_1)t)}, e^{i((2k_2-k_1)X-(2\omega_2-\omega_1)t)}, e^{i((k_2+2k_1)X-(\omega_2+2\omega_1)t)}, e^{i((k_2-2k_1)X-(\omega_2-2\omega_1)t)},$$

$$e^{i((2k_{2+m}+k_1)X-(2\omega_2+2\omega_m+\omega_1)t)}, e^{i((2k_{2+m}-k_1)X-(2\omega_2+2\omega_m-\omega_1)t)}, e^{i((k_{2+m}+2k_1)X-(\omega_2+\omega_m+2\omega_1)t)},$$

$$e^{i((k_{2+m}-2k_1)X-(\omega_2+\omega_m-2\omega_1)t)}, e^{i((2k_{2-m}+k_1)X-(2\omega_2-2\omega_m+\omega_1)t)}, e^{i((2k_{2-m}-k_1)X-(2\omega_2-2\omega_m-\omega_1)t)},$$

$$e^{i((k_{2-m}+2k_1)X-(\omega_2-\omega_m+2\omega_1)t)}, e^{i((k_{2-m}-2k_1)X-(\omega_2-\omega_m-2\omega_1)t)}, e^{i((k_2+k_{2+m}+k_1)X-(2\omega_2+\omega_m+\omega_1)t)},$$

$$e^{i((k_2+k_{2+m}-k_1)X-(2\omega_2+\omega_m-\omega_1)t)}, e^{i((k_2-k_{2m}k_1)X-(-\omega_m\omega_1)t)}, e^{i((k_2-k_{2+m}-k_1)X-(-\omega_m-\omega_1)t)},$$

$$e^{i((-k_2+k_{2+m}+k_1)X-(\omega_m+\omega_1)t)}, e^{i((-k_2+k_{2+m}-k_1)X-(\omega_m-\omega_1)t)}, e^{i((k_2+k_{2-m}+k_1)X-(2\omega_2-\omega_m+\omega_1)t)}$$

$$e^{i((k_2+k_{2-m}-k_1)X-(2\omega_2-\omega_m-\omega_1)t)}, e^{i((k_2-k_{2-m}+k_1)X-(\omega_m+\omega_1)t)}, e^{i((k_2-k_{2-m}-k_1)X-(\omega_m-\omega_1)t)},$$

$$e^{i((-k_2+k_{2-m}+k_1)X-(-\omega_m+\omega_1)t)}, e^{i((-k_2+k_{2-m}-k_1)X---\omega_m-\omega_1)t}, e^{i((k_{2+m}+k_{2-m}+k_1)X-(2\omega_2+\omega_1)t)},$$

$$e^{i((k_{2+m}+k_{2-m}-k_1)X-(2\omega_2-\omega_1)t)}, e^{i((k_{2+m}-k_{2-m}+k_1)X-(2\omega_m+\omega_1)t)}, e^{i((k_{2+m}-k_{2-m}-k_1)X-(2\omega_m-\omega_1)t)},$$

$$e^{i((-k_{2+m}+k_{2-m}+k_1)X-(-2\omega_m+\omega_1)t)}, e^{i((-k_{2+m}+k_{2-m}-k_1)X-(-2\omega_m-\omega_1)t)}.$$

Similarly, the nonlinear driving stress $\mathbf{S}^{\mathbf{NL}}$ in the counter mixing case is evaluated. In this case, the equation of the modulated wave is still referred to Eq. (2) while the single-frequency wave equation is modified as

$$\mathbf{u}_1(\boldsymbol{X}, \boldsymbol{Y}, \boldsymbol{Z}) = \boldsymbol{A}_1 \mathbf{U}_1(\boldsymbol{Z}) \mathbf{e}^{\mathbf{i}(-k_1 X-\omega_1 t)} + c.c. \tag{A1}$$

The terms associated with quadratic nonlinearity include these combinations:

$$\mathbf{e}^{\mathbf{i}((k_2-k_1)X-(\omega_2+\omega_1)t)}, \mathbf{e}^{\mathbf{i}((k_2+k_1)X-(\omega_2-\omega_1)t)}, \mathbf{e}^{\mathbf{i}((k_{2+m}-k_1)X-(\omega_2+\omega_m+\omega_1)t)}, \mathbf{e}^{\mathbf{i}((k_{2+m}+k_1)X-(\omega_2+\omega_m-\omega_1)t)},$$

$$\mathbf{e}^{\mathbf{i}((k_{2-m}-k_1)X-(\omega_2-\omega_m+\omega_1)t)}, \mathbf{e}^{\mathbf{i}((k_{2-m}+k_1)X-(\omega_2-\omega_m-\omega_1)t)}, \mathbf{e}^{\mathbf{i}(-(k_2-k_1)X+(\omega_2+\omega_1)t)}, \mathbf{e}^{\mathbf{i}(-(k_2+k_1)X+(\omega_2-\omega_1)t)},$$

$$\mathbf{e}^{\mathbf{i}(-(k_{2+m}-k_1)X+(\omega_2+\omega_m+\omega_1)t)}, \mathbf{e}^{\mathbf{i}(-(k_{2+m}+k_1)X+(\omega_2+\omega_m-\omega_1)t)}, \mathbf{e}^{\mathbf{i}(-(k_{2-m}-k_1)X+(\omega_2-\omega_m+\omega_1)t)},$$

$$\mathbf{e}^{\mathbf{i}(-(k_{2-m}+k_1)X+(\omega_2-\omega_m-\omega_1)t)}.$$

The terms corresponding to the cubic nonlinearity have the following combinations with the terms corresponding to the CMCs underlined:

$$e^i((2k_2-k_1)X-(2\omega_2+\omega_1)t), e^i((2k_2+k_1)X-(2\omega_2-\omega_1)t), e^i((k_2-\omega 2k_1)X-(\omega_2+2\omega_1)t), e^i((k_2+2k_1)X-(\omega_2-2\omega_1)t),$$

$$\mathbf{e}^{\mathbf{i}((2k_{2+m}-k_1)X-(2\omega_2+2\omega_m+\omega_1)t)}, \mathbf{e}^{\mathbf{i}((2k_{2+m}+k_1)X-(2\omega_2+2\omega_m-\omega_1)t)}, \mathbf{e}^{\mathbf{i}((k_{2+m}-2k_1)X-(\omega_2+\omega_m+2\omega_1)t)},$$

$$\mathbf{e}^{\mathbf{i}((k_{2+m}+2k_1)X-(\omega_2+\omega_m-2\omega_1)t)}, \mathbf{e}^{\mathbf{i}((2k_{2-m}-k_1)X-(2\omega_2-2\omega_m+\omega_1)t)}, \mathbf{e}^{\mathbf{i}((2k_{2-m}+k_1)X-(2\omega_2-2\omega_m-\omega_1)t)},$$

$$\mathbf{e}^{\mathbf{i}((k_{2-m}-2k_1)X-(\omega_2-\omega_m+2\omega_1)t)}, \mathbf{e}^{\mathbf{i}((k_{2-m}+2k_1)X-(\omega_2-\omega_m-2\omega_1)t)}, \mathbf{e}^{\mathbf{i}((k_2+k_{2+m}-k_1)X-(2\omega_2+\omega_m+\omega_1)t)},$$

$$e^{i}((k_2+k_{2+m}+k_1)X-(2\omega_2+\omega_m-\omega_1)t), e^{i}((k_2-k_2m-k_1)X-(\omega-\omega_m\omega_1)t), e^{i}((k_2-k_2mk_1)X-(\omega-\omega_m-\omega_1)t)$$

$$\mathbf{e}^{\mathbf{i}((-k_2+k_{2+m}-k_1)X-(\omega_m+\omega_1)t)}, \mathbf{e}^{\mathbf{i}((-k_2+k_{2+m}+k_1)X-(\omega_m-\omega_1)t)}, \mathbf{e}^{\mathbf{i}((k_2+k_{2-m}-k_1)X-(2\omega_2-\omega_m+\omega_1)t)},$$

$$\mathbf{e}^{\mathbf{i}((k_2+k_{2-m}+k_1)X-(2\omega_2-\omega_m-\omega_1)t)}, \mathbf{e}^{\mathbf{i}((k_2-k_{2-m}-k_1)X-(\omega_m\pm\omega_1)t)}, \mathbf{e}^{\mathbf{i}((k_2-k_{2-m}+k_1)X-(\omega_m-\omega_1)t)},$$

$$\mathbf{e}^{\mathbf{i}((-k_2+k_{2-m}-k_1)X-(-\omega_m+\omega_1)t)}, \mathbf{e}^{\mathbf{i}((-k_2+k_{2-m}+k_1)X---\omega_m-\omega_1)t}, \mathbf{e}^{\mathbf{i}((k_{2+m}+k_{2-m}-k_1)X-(2\omega_2+\omega_1)t)},$$

$$\mathbf{e}^{\mathbf{i}((k_{2+m}+k_{2-m}+k_1)X-(2\omega_2-\omega_1)t)}, \mathbf{e}^{\mathbf{i}((k_{2+m}-k_{2-m}-k_1)X-(2\omega_m+\omega_1)t)}, \mathbf{e}^{\mathbf{i}((k_{2+m}-k_{2-m}+k_1)X-(2\omega_m-\omega_1)t)},$$

$$\mathbf{e}^{\mathbf{i}((-k_{2+m}+k_{2-m}-k_1)X-(-2\omega_m+\omega_1)t)}, \mathbf{e}^{\mathbf{i}((-k_{2+m}+k_{2-m}+k_1)X-(-2\omega_m-\omega_1)t)}.$$

References

[1] K.Y. Jhang, Nonlinear ultrasonic techniques for nondestructive assessment of micro damage in material: a review, Int. J. Precis. Eng. Manuf. 10 (2009) 123–135, https://doi.org/10.1007/s12541-009-0019-y.

[2] V. Zaitsev, Nonlinear acoustics in studies of structural features of materials, MRS Bull. 44 (2019) 350–360, https://doi.org/10.1557/mrs.2019.109.

[3] V.K. Chillara, C.J. Lissenden, Review of nonlinear ultrasonic guided wave nondestructive evaluation: theory, numerics, and experiments, Opt. Eng. 55 (2015), 011002, https://doi.org/10.1117/1.OE.55.1.011002.

[4] K.H. Matlack, J.Y. Kim, L.J. Jacobs, J. Qu, Review of second harmonic generation measurement techniques for material state determination in metals, J. Nondestruct. Eval. 34 (2015) 273, https://doi.org/10.1007/s10921-014-0273-5.

[5] C.J. Lissenden, Nonlinear ultrasonic guided waves—Principles for nondestructive evaluation, J. Appl. Phys. 129 (2021), 021101, https://doi.org/10.1063/5.0038340.

[6] V. Marcantonio, D. Monarca, A. Colantoni, M. Cecchini, Ultrasonic waves for materials evaluation in fatigue, thermal and corrosion damage: a review, Mech. Syst. Sig. Process. 120 (2019) 32–42, https://doi.org/10.1016/j.ymssp.2018.10.012.

[7] C. Yeung, C.T. Ng, Nonlinear guided wave mixing in pipes for detection of material nonlinearity, J. Sound Vib. 485 (2020), 115541, https://doi.org/10.1016/j.jsv.2020.115541.

[8] M.X. Deng, J. Yang, Characterization of elastic anisotropy of a solid plate using nonlinear Lamb wave approach, J. Sound Vib. 308 (2007) 201–211, https://doi.org/10.1016/j.jsv.2007.07.029.

[9] W. Li, B. Chen, Y. Cho, Nonlinear feature of phase matched Lamb waves in solid plate, Appl. Acoust. 160 (2020), 107124, https://doi.org/10.1016/j.apacoust.2019.107124.

[10] G. Gao, C. Liu, N. Hu, M. Deng, H. Chen, Y. Xiang, Response of second-harmonic generation of Lamb wave propagation to microdamage thickness in a solid plate, Wave Motion 96 (2020), 102557, https://doi.org/10.1016/j.wavemoti.2020.102557.

[11] A. Srivastava, F.L. di Scalea, On the existence of antisymmetric or symmetric Lamb waves at nonlinear higher harmonics, J. Sound Vib. 323 (2009) 932–943, https://doi.org/10.1016/j.jsv.2009.01.027.

[12] Y. Ishii, S. Biwa, T. Adachi, Non-collinear interaction of guided elastic waves in an isotropic plate, J. Sound Vib. 419 (2018) 390–404, https://doi.org/10.1016/j.jsv.2018.01.031.

[13] A.K. Metya, S. Tarafder, K. Balasubramaniam, Nonlinear Lamb wave mixing for assessing localized deformation during creep, NDT E Int. 98 (2018) 89–94, https://doi.org/10.1016/j.ndteint.2018.04.013.

[14] M. Osika, A. Ziaja-Sujdak, R. Radecki, L. Cheng, W. Staszewski, Nonlinear modes in shear horizontal wave propagation–analytical and numerical analysis, J. Sound Vib. 540 (2022), 117247, https://doi.org/10.1016/j.jsv.2022.117247.

[15] M. Deng, Analysis of second-harmonic generation of Lamb modes using a modal analysis approach, J. Appl. Phys. 94 (2003) 4152–4159, https://doi.org/10.1063/1.1601312.

[16] W. De Lima, M. Hamilton, Finite-amplitude waves in isotropic elastic plates, J. Sound Vib. 265 (2003) 819–839, https://doi.org/10.1016/S0022-460X(02)01260-9.

[17] Y. Liu, V.K. Chillara, C.J. Lissenden, On selection of primary modes for generation of strong internally resonant second harmonics in plate, J. Sound Vib. 332 (2013) 4517–4528, https://doi.org/10.1016/j.jsv.2013.03.021.

[18] W. Zhu, Y. Xiang, C.J. Liu, M. Deng, F.Z. Xuan, A feasibility study on fatigue damage evaluation using nonlinear Lamb waves with group-velocity mismatching, Ultrasonics 90 (2018) 18–22, https://doi.org/10.1016/j.ultras.2018.06.002.

[19] C. Pruell, J.Y. Kim, J. Qu, L. Jacobs, A nonlinear-guided wave technique for evaluating plasticity-driven material damage in a metal plate, Ndt E Int. 42 (2009) 199–203, https://doi.org/10.1016/j.ndteint.2008.09.009.

[20] W. Li, Y. Cho, Thermal fatigue damage assessment in an isotropic pipe using nonlinear ultrasonic guided waves, Exp. Mech. 54 (2014) 1309–1318, https://doi.org/10.1007/s11340-014-9882-2.

[21] Y. Liu, V.K. Chillara, C.J. Lissenden, J.L. Rose, Third harmonic shear horizontal and Rayleigh Lamb waves in weakly nonlinear plates, J. Appl. Phys. 114 (2013), 114908, https://doi.org/10.1063/1.4821252.

[22] S. Shan, L. Cheng, Mixed third harmonic shear horizontal wave generation: interaction between primary shear horizontal wave and second harmonic Lamb wave, Smart Mater. Struct. 28 (2019), 085042, https://doi.org/10.1088/1361-665X/ab1fce.

[23] S. Gebrekidan, T. Kang, H.J. Kim, S.J. Song, Nonlinear ultrasonic characterization of early degradation of fatigued Al6061-T6 with harmonic generation technique, Ultrasonics 85 (2018) 23–30, https://doi.org/10.1016/j.ultras.2017.12.011.

[24] F. Wen, S. Shan, L. Cheng, Third harmonic shear horizontal waves for material degradation monitoring, Struct.Health Monit. 20 (2021) 475–483, https://doi.org/10.1177/1475921720936983.

[25] S. Shan, L. Cheng, P. Li, Adhesive nonlinearity in Lamb-wave-based structural health monitoring systems, Smart Mater. Struct. 26 (2016), 025019, https://doi.org/10.1088/1361-665X/26/2/025019.
[26] Y. Tian, Y. Shen, D. Rao, W. Xu, Metamaterial improved nonlinear ultrasonics for fatigue damage detection, Smart Mater. Struct. 28 (2019), 075038, https://doi.org/10.1088/1361-665X/ab2566.
[27] J. Jiao, X. Meng, C. He, B. Wu, Nonlinear Lamb wave-mixing technique for micro-crack detection in plates, NDTE Int. 85 (2017) 63–71, https://doi.org/10.1016/j.ndteint.2016.10.006.
[28] X. Ding, Y. Zhao, M. Deng, G. Shui, N. Hu, One-way Lamb mixing method in thin plates with randomly distributed micro-cracks, Int. J. Mech. Sci. 171 (2020), 105371, https://doi.org/10.1016/j.ijmecsci.2019.105371.
[29] S. Sampath, H. Sohn, Non-contact microcrack detection via nonlinear Lamb wave mixing and laser line arrays, Int. J. Mech. Sci. 237 (2023), 107769, https://doi.org/10.1016/j.ijmecsci.2022.107769.
[30] M. Hasanian, C.J. Lissenden, Second order harmonic guided wave mutual interactions in plate: vector analysis, numerical simulation, and experimental results, J. Appl. Phys. 122 (2017), 084901, https://doi.org/10.1063/1.4993924.
[31] M. Hasanian, C.J. Lissenden, Second order ultrasonic guided wave mutual interactions in plate: arbitrary angles, internal resonance, and finite interaction region, J. Appl. Phys. 124 (2018), 164904, https://doi.org/10.1063/1.5048227.
[32] S. Shan, M. Hasanian, H. Cho, C.J. Lissenden, L. Cheng, New nonlinear ultrasonic method for material characterization: codirectional shear horizontal guided wave mixing in plate, Ultrasonics 96 (2019) 64–74, https://doi.org/10.1016/j.ultras.2019.04.001.
[33] J. Jiao, H. Lv, C. He, B. Wu, Fatigue crack evaluation using the non-collinear wave mixing technique, Smart Mater. Struct. 26 (2017), 065005, https://doi.org/10.1088/1361-665X/aa6c43.
[34] S. Sampath, H. Sohn, Cubic nonlinearity parameter measurement and material degradation detection using nonlinear ultrasonic three-wave mixing, Ultrasonics 121 (2022), 106670, https://doi.org/10.1016/j.ultras.2021.106670.
[35] S. Sampath, H. Sohn, Detection and localization of fatigue crack using nonlinear ultrasonic three-wave mixing technique, Int. J. Fatigue 155 (2022), 106582, https://doi.org/10.1016/j.ijfatigue.2021.106582.
[36] V.Y. Zaitsev, V. Gusev, B. Castagnede, Observation of the “Luxemburg–Gorky effect” for elastic waves, Ultrasonics 40 (2002) 627–631, https://doi.org/10.1016/s0041-624x(02)00187-7.
[37] V. Zaitsev, V. Gusev, B. Castagnede, Luxemburg-Gorky effect retooled for elastic waves: a mechanism and experimental evidence, Phys. Rev. Lett. 89 (2002), 105502, https://doi.org/10.1103/PhysRevLett.89.105502.
[38] V. Zaitsev, V. Nazarov, V. Gusev, B. Castagnede, Novel nonlinear-modulation acoustic technique for crack detection, NDT E Int. 39 (2006) 184–194, https://doi.org/10.1016/j.ndteint.2005.07.007.
[39] V.Y. Zaitsev, V. Nazarov, V. Tournat, V. Gusev, B. Castagnede, Luxemburg-Gorky effect in a granular medium: probing perturbations of the material state via cross-modulation of elastic waves, Europhys. Lett. 70 (2005) 607, https://doi.org/10.1209/epl/i2005-10023-5.
[40] B.D.H. Tellegen, Interaction between radio-waves? Nature 131 (1933) 840, https://doi.org/10.1038/131840a0.
[41] A. Garrett, Kinetic theory of cross-modulation in a weakly ionized plasma, J. Plasma Phys. 46 (1991) 365–390, https://doi.org/10.1017/S0022377800016196.
[42] V. Bailey, D. Martyn, The influence of electric waves on the ionosphere, Philos. Mag. 18 (1934) 369–386, https://doi.org/10.1080/14786443409462506.
[43]] V.L. Ginzburg, To the theory of the Luxemburg–Gorky effect, Izvestia Acad. Sci. 12 (1948) 253. USSR, Ser. Phys.Russian.
[44] F. Aymerich, W. Staszewski, Experimental study of impact-damage detection in composite laminates using a cross-modulation vibro-acoustic technique, Struct. Health Monit. 9 (2010) 541–553, https://doi.org/10.1177/1475921710365433.
[45] Y. Wang, J.D. Achenbach, Interesting effects in harmonic generation by plane elastic waves, Acta Mech. Sin. 33 (2017) 754–762, https://doi.org/10.1007/s10409-017-0676-5.
[46] F. Wen, S. Shan, R. Radecki, W.J. Staszewski, L. Cheng, Shear-lag modelling of surface-bonded magnetostrictive transducers for shear horizontal wave generation in a non-ferromagnetic plate, Smart Mater. Struct. 30 (2021), 035026, https://doi.org/10.1088/1361-665X/abe183.